Catalysis Science & Technology

ROYAL SOCIETY OF CHEMISTRY

PAPER

View Article Online
View Journal | View Issue

Cite this: *Catal. Sci. Technol.*, 2021, **11**, 1077

Role of Ga^{3+} promoter in the direct synthesis of iso-butanol *via* syngas over a K–ZnO/$ZnCr_2O_4$ catalyst†

Tao Zhang,[a] Chunyang Zeng,[b] Yingquan Wu,[a] Nana Gong,[ac] Jiaqian Yang,[ac] Guohui Yang,[a] Noritatsu Tsubaki *[d] and Yisheng Tan *[a]

Received 28th August 2020,
Accepted 26th November 2020

DOI: 10.1039/d0cy01688h

rsc.li/catalysis

The direct synthesis of iso-butanol is an important reaction in syngas (composed of CO and H_2) conversion. K–ZnO/$ZnCr_2O_4$ (K–ZnCr) is a commonly used catalyst. Here, Ga^{3+} is used as an effective promoter to boost the efficiency of the catalyst and retard the production of CO_2. X-ray diffraction, X-ray photoelectron spectroscopy, ultraviolet-visible diffuse reflection spectroscopy and electron microscopy were used to characterize the structural variations with different amounts of Ga^{3+}, the results showed that the particle size of the catalyst decreases with the addition of Ga^{3+}. The temperature-programmed desorption of NH_3 and CO_2, and diffuse reflectance infrared Fourier-transform spectroscopy (DRIFTs) analysis of the CO adsorption revealed that the acidity and basicity were altered owing to the different forms of Ga^{3+} adoption. X-ray photoelectron spectroscopy and density functional theory (DFT) calculations revealed that the formation of Ga clusters that are coordinated on the exposed surfaces of $ZnCr_2O_4$, and undergo a tetra-coordinated Ga^{3+} exchange with one of the Zn in $ZnCr_2O_4$ (ZG) and $ZnGa_2O_4$, probably depends on the amount of Ga added. The structural evolution of the Ga^{3+} promoted K–ZnO/$ZnCr_2O_4$ catalysts can be described as follows: (i) the main forms are ZG and Ga coordinated $ZnCr_2O_4$, in which the amount of Ga^{3+} is below 1.10 wt%; and (ii) the Ga^{3+} containing compound is gradually changed from ZG to $ZnGa_2O_4$ and the amount of gallium clusters increased when the amount of Ga^{3+} was higher than 1.10 wt%. The catalytic performance evaluation results show that K–$Ga_{1.10}$ZnCr exhibits the highest space time yield and selectivity of alcohols, in which the three compounds play different roles in syngas conversion: ZG is the main active site that boosts the efficiency of the catalysts, owing to the intensified CO adsorption and decreased activation energy of CHO formation through CO hydrogenation; $ZnGa_2O_4$ only modifies the surface basicity and acidity on the catalyst, thereby impacting the carbon chain growth after the CO is adsorbed. The effects of Ga coordinated with $ZnCr_2O_4$ shows little impact on the CO adsorption owing to the weak electron donating effects of Ga.

Introduction

The increasing demand for clean fuel has ignited research on converting carbon containing substances to fuel or valuable chemicals.[1] Syngas, mainly composed of H_2 and CO, is usually obtained through the gasification of coal or biomass or is produced by methane and CO_2 reforming, and is an important platform material for producing gasoline, diesel oil and many valuable chemicals.[2] Iso-butanol is an important chemical among all of the downstream products of syngas and can be used as a gasoline additive to improve the octane number.[3,4] In addition, iso-butanol can also be used to purify rare earth or produce important chemicals.[5] However, until now, the main production route of iso-butanol is the carbonylation of propylene and fermentation of sugar.[4,5] Hence, it is urgent to produce iso-butanol using an alternative approach.

Direct synthesis of iso-butanol through syngas has been proven to be an effective method owing to the wide usage of carbon containing substances and the high selectivity of iso-butanol.[4,6,7] Among all of the catalysts, the K–ZnO/$ZnCr_2O_4$ (K–ZnCr) catalyst is considered to be a good candidate owing to its longer life time and reduced CO_2 emissions.[4,8,9] To determine the reaction mechanism of the K–ZnCr catalyst, researchers performed a lot of work to disclose the structure–property relationships. For instance, Tian *et al.* proposed that

[a] *State Key Laboratory of Coal Conversion, Institute of Coal Chemistry, Chinese Academy of Science, Taiyuan, Shanxi 030001, China. E-mail: tan@sxicc.ac.cn*
[b] *China Petroleum Chemical Industry Federation, Beijing 100723, China*
[c] *University of Chinese Academy of Science, Beijing 100049, China*
[d] *Department of Applied Chemistry, School of Engineering, University of Toyama, Gofuku 3190, Toyama, 930-8555, Japan. E-mail: tsubaki@eng.u-toyama.ac.jp*

† Electronic supplementary information (ESI) available. See DOI: 10.1039/d0cy01688h

the non-stoichiometry ZnCr spinel is the active site that produces iso-butanol, and this so-called non-stoichiometry structure is constructed by the disorder of Zn^{2+} and Cr^{3+} in a spinel crystal cell.[8,10,11] Gao *et al.* enhanced the performance of the catalyst by modulating the configuration and the amount of ZnO.[12–14] In addition to the studies on the structure activity performance of the ZnCr catalyst, other researchers also attempted to explore the reaction mechanism of alcohol formation. For example, K. J. Smith *et al.* revealed that the selectivity of methanol and iso-butanol is controlled by the activity of an α- or β-carbon atom of the growing alcohol.[15] Lietti *et al.* investigated the complex reaction network of higher alcohol synthesis by studying the temperature-programmed reaction of C_3, C_4, and C_5 oxygenates over the K-promoted ZnCr catalyst.[16] Inspired by this research, Wu *et al.* explored the rate-determining step of iso-butanol formation and found that the formation of C_2 oxygenates through CO and formyl (CHO) is the key step to controlling the reaction atmosphere and enriching the intermediate alcohols.[5,17]

Based on the reaction mechanism, some researchers have made numerous efforts to further promote the efficiency of the ZnCr catalyst by adding promoters. For example, Epling *et al.* added Pd and Mn to boost the selectivity of iso-butanol and alcohols under the reaction conditions of 10 MPa and 430 °C on a Cs-promoted ZnCr catalyst.[18–21] However, until now, a systematic study concentrated on the influence of the third composition on the structure of the ZnCr iso-butanol catalyst has not been reported. Moreover, among all these investigations, the amount of CO_2 in the tail gas is relatively high. Therefore, reducing the amount of CO_2 emissions during iso-butanol synthesis is also an important issue.

In recent years, Ga^{3+} has been used as a promoter to modulate the electron properties, textural properties, configurations and distribution of the active site composition of Co, Co/AC, CuAl, and CuZnAl catalysts to further modify the activation of CO during the synthesis of alcohols.[6,22–25] In addition, Ga^{3+} can also be used to modulate the efficiency of the water–gas-shift reaction or to improve the performance of CO_2 conversion by altering the acid–base properties of the catalyst.[26–28] However, when Ga was introduced into the Zn containing catalyst, the existing form of Ga and its effect on the performance of the catalyst was still conflicting. For example, Meng-Jung Li *et al.* proposed that the formation of $ZnGa_2O_4$ creates an electronic heterojunction with excess ZnO to facilitate the reduction of Zn^{2+} to Zn in the CuZnO methanol catalyst.[27] Ham *et al.* confirmed that the phase transformation of gallium oxide from tetrahedral Ga–O sites to octahedral Ga–O sites suppressed the formation of dimethyl ether (DME).[29] At present, whether the catalytic performance of K–ZnCr is promoted by the introduction of Ga^{3+} is not clear based on our knowledge. In addition, the form of Ga^{3+}, its impact on the structure of the catalyst and the explicit role it plays during the reaction are still unknown. To unravel the above-mentioned problems, Ga^{3+} was added into a K–ZnCr iso-butanol catalyst to modulate the surface structure through the formation of novel compounds to further improve the performance of the catalyst.

Experimental section

2.1 Catalyst preparation

Ga^{3+} promoted K–ZnCr catalysts were prepared by precipitation–impregnation. The precursors for Zn, Cr and Ga are zinc nitrate hexahydrate, chromium nitrate nine-hydrate and gallium nitrate hydrate, respectively. In a typical procedure, aqueous solutions of $Zn(NO_3)_2{\cdot}6H_2O$ and $Cr(NO_3)_3{\cdot}9H_2O$ (molar ratio of Zn : Cr = 1 : 1) were precipitated with $(NH_4)_2CO_3$ aqueous solution. The detailed procedure is described in our previous report.[30] The precipitate was dried at 100 °C for 12 h, then milled into a powder and impregnated with the aqueous solution of gallium nitrate hydrate, then dried at 100 °C for 12 h and calcined at 400 °C in a muffle furnace under a steady atmosphere for 4 h to obtain the GaZnCr samples. Finally, the GaZnCr samples were impregnated with the aqueous solution of K_2CO_3, then dried and calcined according to the process of preparing GaZnCr to obtain the final catalysts, the samples can be abbreviated as K–GaZnCr. The amount of Ga (mole fraction) is changed from 0, 0.55 1.10, 1.64, to 2.18 wt%, respectively. The final catalysts were denoted as K–Ga_xZnCr, in which x represents the loading amount of Ga.

2.2 Catalyst evaluation for iso-butanol synthesis

The performance of the catalysts was evaluated in a fixed-bed tubular reactor, composed of a titanium alloy tube (Φ10 × 2 × 400 mm) inserted into a furnace. 1.0 g of the catalyst with a particle size of 50 to 60 mesh was packed, and the two ends were stuffed with quartz sand to support the catalyst. Before introducing syngas, the catalyst was reduced using 10% H_2 in N_2 with a flow rate of 100 mL h^{-1} at 400 °C for 6 h. After reduction, syngas with a molar ratio of H_2/CO = 2.4 was introduced into the reactor. The reaction conditions were as follows: pressure 10.0 MPa, gas hourly space velocity (GHSV) 3300 h^{-1} and a reaction temperature of 400 °C. The detailed procedures for sample collection, the composition analysis of syngas, tail gas and the liquid phase are described in our previous report.[11,30]

2.3 Characterization

The specific surface face areas were obtained according to the Brunauer–Emmett–Teller (BET) method using nitrogen adsorption and desorption isotherms at −196 °C on ASAP 2020 V4.03 equipment. Before the test, each sample was degassed at 200 °C for 4 h. The morphology and microstructure of the catalysts were investigated using high resolution transmission electron microscopy (HRTEM, JEM-2100F) operated at 200 kV (produced by Japan Electronics Co., Ltd). The X-ray diffraction (XRD) data for the K–Ga_xZnCr catalysts were recorded using a D8 Advance X-ray diffractometer in the 2θ range from 10° to 80° with Cu Kα

radiation. To obtain a spectrum with high quality, the scanning step size and speed were set to 0.01 and 1° min^{-1}, respectively. The X-ray photoelectron spectroscopy (XPS) patterns were recorded using an AXIS ULTRA DLD X-ray photoelectron spectrometer equipped with a multichannel detector. Charge referencing was performed against adventitious carbon (C 1s, 284.8 eV). A Shirley-type background was subtracted from the signals. The recorded spectra were fitted using Gaussian–Lorentzian curves to determine the composition of the surface of the different samples. CO_2 and NH_3 temperature programmed desorption profiles were recorded on a TP-5050 automatic chemical adsorption instrument.

The test temperature is in the range from 50 to 800 °C. The catalyst samples were reduced using a mixture of 10% H_2 and 90% N_2. The reduction was performed at 400 °C for 2.5 h with a heating rate of 10 °C min^{-1}. After reduction, the samples were cooled to 50 °C under the protection of 10% H_2 and 90% N_2. Then, the catalysts were treated in a constant flow of N_2 with a rate of 30 mL min^{-1} to eliminate the physically adsorbed water and contaminates. After that, NH_3 or CO_2 was introduced into the system for 0.5 h to achieve saturated adsorption. The samples were purged with N_2 for about 1 h to remove the physically absorbed NH_3 or CO_2. Finally, the temperature was increased at a rate of 10 °C min^{-1} under an N_2 atmosphere. The signals of CO_2 and NH_3 were recorded by a thermal conductivity detector respectively. X-ray fluorescence (XRF) spectra were recorded using an E3 Tiger XRF spectrometer with a silicon drift detector (SDD). Raman spectra and solid-state UV-visible spectra were also recorded to reveal the influence of the Ga species on the K–Ga_xZnCr catalyst structure. A Raman test was performed using a HORIBA 800 with a 532 nm excitation wavelength. Solid state UV-visible spectrums were recorded in a SU3900 spectrophotometer, the scanning range is from 200 to 800 nm by using barium sulfate as the base.

For the above analysis, BET, XPS, Raman spectra and solid state ultraviolet-visible diffuse reflectance spectrums were performed on the reduced catalyst samples. The composition of the reduction gas and the procedure used was identical to the procedure used before catalyst evaluation.

In addition, the FT-IR spectra of CO adsorption were obtained on a TENSOR-27 in the range of 4000 to 600 cm^{-1} with a 4 cm^{-1} resolution, the detailed procedures for CO adsorption were described in our earlier reports.[30]

Results and discussion

3.1 BET surface areas of the catalysts

The textural parameters of the reduced K–Ga_xZnCr catalysts are listed in Table 1. As shown, the BET areas of the samples regularly changed with the addition of Ga^{3+}, that is 63.86 m^2 g^{-1} for K–Ga_0ZnCr, 78.43 m^2 g^{-1} for K–$Ga_{0.55}$ZnCr, 75.96 m^2 g^{-1} for K–$Ga_{1.10}$ZnCr, 66.54 m^2 g^{-1} for K–$Ga_{1.64}$ZnCr and 61.71 m^2 g^{-1} for K–$Ga_{2.18}$ZnCr, respectively. This phenomenon is also observed when investigating the external surface area. However, as for the change in the average pore diameter and its distributions (Fig. S1†), one can see that the smaller pores were created by Ga^{3+} addition, which is in accordance with the studies performed by Ham *et al.* and Kim *et al.* who discovered an increased surface area and decreased pore diameter when Ga was added to the Cu/*m*-Al_2O_3 catalyst or CuO–Cr_2O_3 water gas shift reaction catalyst.[26,29] With the increase in the BET area, more active sites were created. Therefore a superior performance will be expected from the catalyst. The change in the catalyst texture may be caused by the interaction between the Ga species and ZnCr oxides which alters the morphology of the catalyst. The exact images of the Ga^{3+} doped catalyst are further characterized using HRTEM in the following section.

3.2 HRTEM characterization

The HRTEM images of the K–ZnCr catalyst with and without Ga modification are shown in Fig. S2 and S3.† When comparing the photos of the two samples, one can see that after adding Ga^{3+} to the K–ZnCr catalyst, the particles become smaller. As shown in the histogram, the particle size of the K–Ga_0ZnCr sample is mostly in the range of 5.5 to 6.5 nm, while for the K–$Ga_{1.10}$ZnCr sample, the particle is in the range of 4.5 to 6.5 nm with a uniform distribution. The average particle size decreased from 6.98 nm to 6.11 nm after Ga^{3+} introduction, implying that the microstructure of the K–ZnCr catalyst was altered by Ga^{3+} addition, which is also observed for the Ga doped CoZnAl catalyst.[22] When considering the exposed surface of the K–ZnCr catalyst with or without Ga addition, one can see that the (311), (310) and (202) surfaces of $ZnCr_2O_4$ are the most exposed surfaces after Ga modification. The alteration of the particle sizes and distribution of the crystal surface caused by Ga addition may be attributed to the interaction between Ga^{3+} and ZnCr oxides or the interactions between the Ga cluster and ZnCr

Table 1 BET areas, pore volume and average pore diameter of the K–Ga_xZnCr catalysts (x = 0, 1.5, 3.0, 4.5 and 6.0)

Catalyst	BET area[a] (m^2 g^{-1})	External surface area[b] (m^2 g^{-1})	Pore volume[c] (cm^3 g^{-1})	Average pore diameter[d] (nm)
K–Ga_0ZnCr	63.86	62.89	0.2197	12.08
K–$Ga_{0.55}$ZnCr	78.43	76.67	0.2490	11.48
K–$Ga_{1.10}$ZnCr	75.96	71.90	0.2388	11.35
K–$Ga_{1.64}$ZnCr	66.08	65.77	0.1924	10.46
K–$Ga_{2.18}$ZnCr	61.71	57.42	0.2052	12.75

[a] BET area was calculated by applying the multi-point BET equation in the linear range. [b] *t*-Plot external surface area. [c] Single point adsorption total pore volume at P/P_0 = 0.99. [d] Desorption average pore diameter (4 V/A by BET).

oxides. The explicit form of the Ga^{3+} doped species was verified using XPS analysis and density functional theory (DFT) calculations in the following section. In addition, although the change in the particle sizes is in accordance with the observation of the BET test, the TEM images only gives part of the morphologies of the catalyst samples, the exact particle sizes of the K–Ga_xZnCr samples should be analysed by characterizing the bulk structure of the samples, which will be investigated by analysing the XRD patterns in the subsequent section.

3.3 XRD characterization

The XRD patterns of the catalyst samples with different amounts of added Ga^{3+} are shown in Fig. 1. As shown, all the K–Ga_xZnCr catalysts presented diffraction peaks that were assigned to ZnO and $ZnCr_2O_4$, and no new peaks were observed when Ga^{3+} was introduced, implying the high dispersion of the Ga^{3+} compounds. The particle size of the (310) surfaces of $ZnCr_2O_4$ were calculated using the Scherrer equation and are listed in Fig. 1A. As can be seen, the $ZnCr_2O_4$ particles become much smaller when Ga^{3+} is introduced. This trend is in accordance with the observations from the HRTEM analysis. In addition, to give a better understanding of the impact of Ga^{3+} on ZnO and $ZnCr_2O_4$, a Rietveld refinement was performed using MUAD software.[31–34] The results of the refinement are shown in Fig. S4.† The mass fractions of ZnO and $ZnCr_2O_4$ according to the refinement are listed in Table S1.† As shown, the weight fraction of $ZnCr_2O_4$ increases with the increasing amount of Ga^{3+}, while this trend is opposite for ZnO, indicating that the composition of the K–ZnCr catalyst was altered by the introduction of Ga^{3+}. Furthermore, after 48 h of time-on-stream, it can be observed from the corresponding catalysts that the diffraction peaks of both ZnO and $ZnCr_2O_4$ were intensified (Fig. 1B), implying the growth of the particle size of these two species during the reaction. Gao *et al.* illustrated that the configurations and absorption energy of CO can be altered by the morphology of ZnO owing to its different interactions with the $ZnCr_2O_4$ (111) surface.[12] Based on this discovery, we can deduce that the interaction between ZnO and $ZnCr_2O_4$ can be altered by the addition of Ga^{3+}. This may be caused by the interaction between Ga and $ZnCr_2O_4$, or the formation of other compounds such as $ZnGa_2O_4$ through the respective oxides of gallium, chromium and zinc. In the following section, a thermodynamic calculation was performed to verify the possible transformation process of the Ga species.

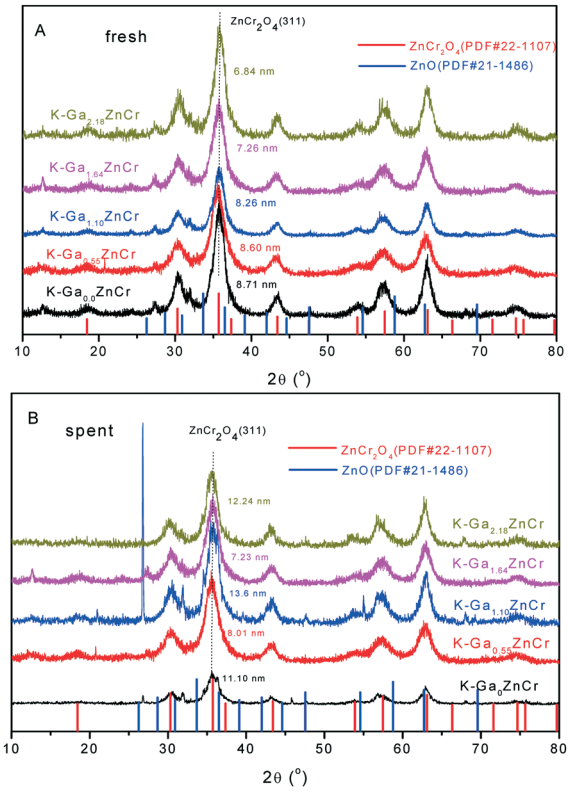

Fig. 1 XRD patterns of the (A) fresh and (B) spent K–Ga_xZnCr catalysts.

3.4 Possible locations of Ga^{3+} calculated using DFT

To deduce the possible locations of Ga^{3+} in the K–ZnCr iso-butanol catalyst, a thermodynamic calculation was performed. When considering interactions between the Ga^{3+} and ZnCr oxides, the following compounds can be formed: (i) gallium oxide; (ii) Ga^{3+} doped ZnO (ZGO); (iii) one of the metals in $ZnCr_2O_4$ is replaced by Ga^{3+} to form a four coordination or six coordination spinel; and (iv) $ZnGa_2O_4$. DFT calculations were performed to deduce the possible locations of Ga^3 (the detailed procedures are listed in the ESI†). If the Zn^{2+} located at the tetrahedral coordination sites in ZnO and $ZnCr_2O_4$ was replaced by Ga^{3+}, the reduced cell parameters of a and c would be expected owing to the smaller ionic radius (0.47 Å for Ga^{3+} *vs.* 0.6 Å for Zn^{2+}). A similar deduction can also be expected if the Cr^{3+} located at the six coordinated sites of $ZnCr_2O_4$ was replaced by Zn^{2+}(0.74 Å for Cr^{3+} *vs.* 0.62 Å for Ga^{3+}). However, an adverse consequence was obtained here (Table S1†). The differences in the cell parameter, c, of $ZnCr_2O_4$ between the speculated result and the results of Rietveld may originate from the cation disordered ZnCr spinel. To further deduce the location of Ga^{3+}, the binding energy E_B and formation energy E_f were calculated based on the optimized structure using a DFT calculation. The configuration of the possible Ga^{3+} doped species and the reaction are shown in Table S2 (ESI†). As shown, the E_B of these compounds follows the order below: ZG > $ZnCr_2O_4$ > $ZnGa_2O_4$ > CG > ZGO > ZnO, implying that ZG is the most stable Ga^{3+} doped ZnCr compound. When Ga^{3+} was added into a ZnCr catalyst, ZG may be one of the most likely to exist forms of the Ga species, rather than ZGO and CG, owing to its higher stability.

In addition to the doping of Ga^{3+} in $ZnCr_2O_4$, other structures may be formed. For example, the unsaturated sites of the $ZnCr_2O_4$ surfaces were coordinated by Ga^{3+} or clusters of Ga species. To verify this speculation, the adsorption of Ga on the most exposed surfaces of $ZnCr_2O_4$, such as (311), (310)

and (202) (obtained through HRTEM) were calculated. Based on the observation and speculation, the interaction between Ga and $ZnCr_2O_4$ was investigated by calculating the adsorption of Ga on the coordination unsaturated sites of the surfaces. The most stable adsorption configurations are listed in Fig. S5.† Bader charge distributions before and after Ga adsorption are also listed in Table S3.† As shown, all the surfaces accept electrons from Ga, the trend is 310 (0.2940) < 311 (0.4092) < 202 (0.7449). Generally, CO is rich in electrons, a stronger adsorption of CO will be created if the surface is electron deficient. Therefore, a reverse CO adsorption could be expected. The calculated adsorption energies and configurations of CO (Table S4 and Fig. S19†) support this conjecture.

Furthermore, except for the above observed surfaces, there may be lots of possible step surfaces owing to the fact that the surfaces of the particles are very uneven, which could be attributed to the other reaction sites for CO hydrogenation. To better analyse the structure and their effects on syngas conversion, more detailed characterization and computational work should be carried out. Owing to the complexity of the catalyst surface, these configurations are not easy to investigate using DFT calculations. Therefore the DFT calculation shown above gives only part of the functions of the particular structure. However, this approach could be used as a simplified method to study the real surface. In future studies, we will attempt to investigate the structure and function of these step surfaces.

3.5 Raman analysis of the K–Ga$_x$ZnCr catalysts

Raman peaks for the reduced K–Ga$_x$ZnCr samples with an excitation wavelength of 532 nm are shown in Fig. 2. The peaks located at 392 and 900 nm are the characteristic bands for the normal vibration modes of the ZnO and Cr atoms in the tetrahedral and octahedral sites formed by the oxygen atoms.[35] The peaks located at 511 and 605 nm represent the vibration of F_{2g} for $ZnCr_2O_4$ and 680 nm is assigned to the symmetric Cr–O stretching vibration of the A_{1g} symmetry originating from the CrO_6 groups of the spinel.[36,37] The bands at around 846, 867 and 933 nm are ascribed to the Cr═O stretching vibration in the chromate compound.[36] The peak located at 350 nm belongs to the vibration mode associated with the multiple-phonon scattering processes of ZnO.[38] Based on the observation, one can see that the vibrations of ZnO, $ZnCr_2O_4$ and chromate were all weakened after the introduction of Ga^{3+}. Furthermore, for all the samples, the peaks located at 770 and 500 nm, corresponding to the asymmetric stretching of the Ga–O bond in the tetrahedral sites, shows almost the same intensity with an enhanced amount of Ga^{3+}.[39] However, the typical Raman vibration mode that is ascribed to β-Ga_2O_3 was not observed.[39] Moreover, the peaks at 601 and 712 nm that were assigned to the T_{2g} and A_{1g} modes of $ZnGa_2O_4$ were intensified by increasing the amount of Ga^{3+}.[40] This may be the consequence of the interactions between the ZnCr oxides with Ga. With the gradual increase in the amount of Ga^{3+}, the extra ZnO was reacted with Ga_2O_3 to form $ZnGa_2O_4$, Zn located in the tetrahedral site of $ZnCr_2O_4$ was partly replaced by Ga to form a ZG structure which exhausted both ZnO and $ZnCr_2O_4$. In addition, by increasing the amount of Ga^{3+}, chromate was consumed so the intense absorption of chromate vanished. Based on the above mentioned analysis, we may speculate that when a small amount of Ga^{3+} is introduced into the K–ZnCr catalyst, ZG is the dominant structure. However, upon further increasing the amount of Ga^{3+}, the ZnO will react with Ga_2O_3 to form $ZnGa_2O_4$. The surface composition and properties were altered by the different forms of Ga^{3+} species, which need to be confirmed by XPS and chemisorption characterization.

3.6 Ultraviolet-visible diffuse reflectance spectra

An interesting phenomenon for the reduced catalyst samples is the change in the colour of the catalyst, for example K–Ga$_0$ZnCr is a blue-green, upon gradually increasing the amount of Ga^{3+}, the colour becomes increasingly darker. This change was verified by ultraviolet visible diffuse reflectance analysis. As shown in Fig. 3, all the samples absorbed in the range of 200–800 nm, the absorbance of the samples was intensified by increasing the amount of Ga^{3+}. In addition, the diffuse

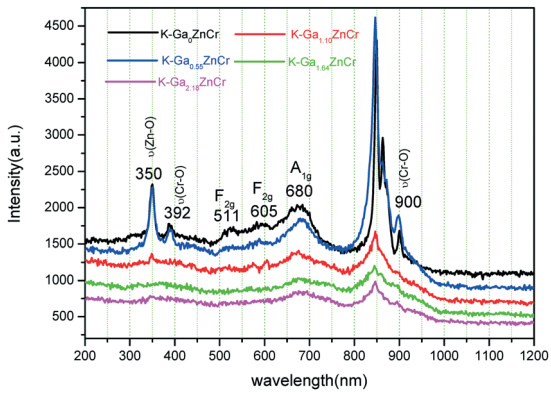

Fig. 2 Raman spectra of the K–GaZnCr catalysts.

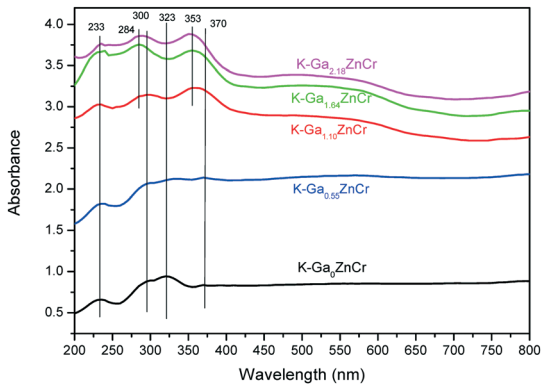

Fig. 3 Ultraviolet-visible diffuse reflectance spectrums of the K–Ga$_x$ZnCr catalysts.

reflectance spectrum gives evidence of the charge transfer of $O^{2-} \rightarrow Zn^{2+}$ in ZnO at 370 nm and in $ZnCr_2O_4$ at 300 nm.[41] The absorption bands at 370 and 260 nm, attributed to the $O^{2-} \rightarrow Cr^{6+}$ charge transfer, were also observed.[41,42] Upon gradually increasing the amount of Ga^{3+}, the absorbance located at 300 nm become overlapped by the emergence of new peaks that were located at 287 and 353 nm, indicating the formation of a new compound, which may be caused by the growth of ZG or Ga^{3+} coordinated on the $ZnCr_2O_4$ surfaces.

Moreover, the indirect band gap energy E_g for the K–Ga_x-ZnCr samples was calculated using the equation $(\alpha h\nu)^2 = C(h\nu - E_g)$ to investigate the influence of Ga addition on the electron structure of the catalysts.[38,43] In the equation, α is the absorption coefficient, $h\nu$ is the photon energy with frequency ν, E_g is the direct band gap energy, and C is a constant. Fig. S6† shows the plot of $(\alpha h\nu)^2$ *versus* $h\nu$. The calculated direct band gap energies for the samples are 2.51 eV for K–Ga_0ZnCr, 2.49 eV for K–$Ga_{0.55}$ZnCr, 1.75 eV for K–$Ga_{1.10}$ZnCr, 2.07 eV for K–$Ga_{1.68}$ZnCr, and 2.03 eV for K–$Ga_{2.18}$ZnCr respectively, which indicates that when Ga was introduced into the K–ZnCr catalyst, the band gap was reduced. Tajizadegan *et al.* observed an E_g value of 1.8 eV for a nanoparticle of $ZnCr_2O_4$ with a particle size of about 17 nm.[44] Huang *et al.* discovered that the E_g of TiO_2 is size dependent, the band gap decreased from 3.239 to 3.173 eV when the particle size decreased from 29 to 17 nm and then increased from 3.173 to 3.289 eV as the particle decreased from 17 to 3.8 nm.[45] Based on the phenomenon and published research, we deduce that the lower E_g after Ga addition may be caused by the smaller particle size of $ZnCr_2O_4$ observed using TEM and XRD. In addition, the coordination of Ga on the exposed oxygen of the $ZnCr_2O_4$ surfaces or the formation of ZG may be another reason that caused the reduced E_g owing to the fact that Ga can donate electrons to $ZnCr_2O_4$.

3.7 Analysis of the surface composition of K–Ga_xZnCr using XPS spectra

The XPS spectra were investigated to disclose the structure evolution process of the K–ZnCr catalyst promoted by Ga^{3+}. The Cr $2p_{3/2}$ and Cr $2p_{1/2}$ spectra of all the samples are listed in Fig. S7.† Four peaks were obtained for each of the samples after deconvoluting the recorded peaks. The binding energy (BE) of 575.75–574.86 eV is the characteristic peak for Cr metal,[46] more specifically, 585.27–579.08 eV and 575.88–576.00 eV are the characteristic peaks of Cr^{3+} (ref. 8 and 11) and 578.49–579.08 eV is the peak of Cr^{6+}.[47] Analysis of the concentration of surface chromium showed that the main composition of surface chromium is Cr^{3+}, the amount of metallic Cr and Cr^{6+} species are only changed in the range of 5.32–12.27% and 5.71–21.21%, respectively (Table S5†), implying that the addition of Ga^{3+} has an obvious impact on the valence state of Cr. In addition, XPS spectra of Zn 2p were also measured. As is shown in Fig. S8,† the BE values of 1020.46–1020.60 eV and 1043.57–1043.68 eV are characteristic of Zn $2p_{1/2}$ and Zn 2p $_{3/2}$, respectively.[37,48,49] The BE of Zn 2p was barely changed with the altered concentration of Ga^{3+}, indicating the similar chemical environment of Zn with and without the introduction of the Ga^{3+} promoter. To further explore the influence of Ga^{3+} addition on the composition of the K–GaZnCr catalyst, XPS analysis of Ga 2p and Ga 3d were performed, and are shown in Fig. 4. The BE at 1116.23–1117.27 eV is the characteristic peak of Ga $2p_{3/2}$, and 1443.06–1143.20 eV is the characteristic peak of Ga $2p_{1/2}$.[49] These values are much smaller than the peaks in K–$ZnGa_2O_4$ and Ga_2O_3 (Fig. S9†), indicating the chemical environment is quite different from pure Ga_2O_3 and K–$ZnGa_2O_4$. In addition, it is obvious that the BE of Ga $2p_{1/2}$ increased from 1143.06 (K–$Ga_{1.10}$ZnCr) to 1143.20 eV (K–$Ga_{2.18}$ZnCr) upon an enhancement of the amount of Ga^{3+}, suggesting the chemical environment of Ga^{3+} was altered by the amount of its usage. To further study the coordination states of Ga^{3+} on the K–GaZnCr catalyst, the Ga $2p_{3/2}$ peaks were deconvoluted into two peaks, the results are shown in Fig. 4D. It can be seen that the Ga^{3+} ions occupy two different coordination sites in the K–GaZnCr: peaks located at 1116–1117 eV, which can be assigned to Ga^{3+} at the tetrahedral sites,[50–52] and the peak at 1117.1–1117.6 eV can be assigned to the Ga^{3+} located at the octahedral sites. In addition, for K–$Ga_{1.10}$ZnCr, the Ga^{3+} located at the tetrahedral sites reaches the maximum value, 74.31%. Another interesting finding is the assignment of Ga $2p_{1/2}$ shown at 1143.06–1143.20 eV. According to Delichere *et al.* the Ga $2p_{1/2}$ for $ZnGa_2O_4$ is located at 1144.3 eV, while for Ga_2O_3 it is 1144.15 eV.[39,48,50,53] The decreased BE of Ga $2p_{1/2}$ may be caused by the formation of the ZG structure or the coordination of the Ga cluster on the surface of $ZnCr_2O_4$, because the electronegativity of Zn and Cr are smaller than that of Ga.[54]

From the above analysis, no remarkable peaks corresponding to Ga_2O_3 were observed owing to the mismatched peaks of the Ga $2p_{3/2}$ and Ga $2p_{1/2}$ spectra for the Ga_2O_3 samples. To further confirm the existing form of Ga^{3+}, the 3d spectra of Ga was performed and the results are shown in Fig. 4E–H. According to Yang *et al.*,[55] Ga is mainly located at the tetrahedral (BE around 21.62) and octahedral sites (BE around 19.93 eV) for all the catalyst samples. The amount of six-coordinated Ga decreased gradually with the increasing amount of Ga added (from 32.52% for K–$Ga_{0.55}$-ZnCr to 22.71% for K–$Ga_{2.18}$ZnCr, Table S6†), and the amount of four-coordinated Ga shows a reversible trend, indicating that different forms of gallium species were formed with different amounts of added Ga^{3+}. This trend is in accordance with the observation of Ga 2p. In addition to the peaks that denote to Ga located at different coordination sites, peaks located at 16.94 to 17.06 eV and 23.37 to 23.85 eV were also observed. The former may be caused by the formation of ZG, while the latter may be the result of gallium clusters or the coordination of Ga to the unsaturated $ZnCr_2O_4$ surfaces.

By fitting the XPS spectrum of Cr 2p, Zn 2p and Ga 2p, the surface concentration of these elements were calculated. As a comparison, the compositions of bulk catalysts were also investigated by XRF analysis. The results are shown in

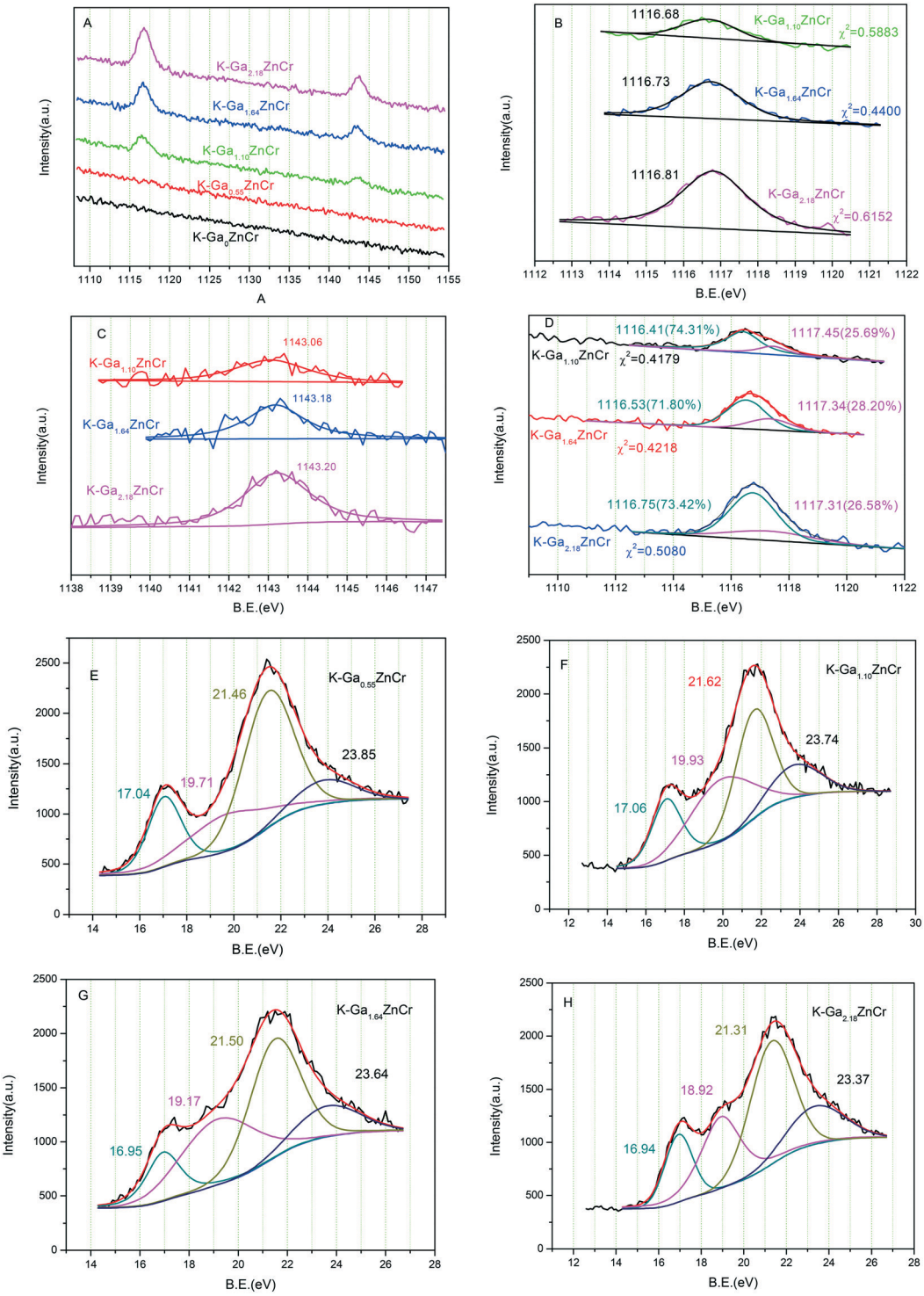

Fig. 4 Ga 2p (A)–(D) and 3d (E)–(H) of the K–Ga$_x$ZnCr samples (x = 0.55, 1.10, 1.64 and 2.18).

Table 2, the molar ratios of Zn/Cr in the bulk for each catalyst are in the range of 0.89 to 0.91, which is smaller than the feed rate. However, on the surface of the catalysts, a remarkable enhancement of Zn was observed. Furthermore, when comparing the ratios of Zn/Ga and Cr/Ga for the bulk and surface, an enhancement of Ga was observed. The enhancement of Zn and Ga on the surface of the catalyst may be ascribed to the interaction of Ga^{3+} with $ZnCr_2O_4$ as discussed in the above section.

To further investigate the structural evolution caused by Ga^{3+} addition, especially the surface oxygen species over Ga promoted catalysts, the O1s XPS spectra of the catalysts were

Table 2 Bulk and surface compositions of Zn, Cr, and Ga for the K–GaZnCr catalysts

Catalysts	Bulk[a]			On the surface[b]		
	Zn/Cr	Zn/Ga	Cr/Ga	Zn/Cr	Zn/Ga	Cr/Ga
K–Ga_0ZnCr	0.94	—	—	1.15	—	—
K–$Ga_{0.55}$ZnCr	0.91	79.82	55.88	1.13	28.03	26.90
K–$Ga_{1.10}$ZnCr	0.91	34.39	23.95	1.12	26.13	23.23
K–$Ga_{1.64}$ZnCr	0.89	22.71	16.12	1.14	17.48	15.64
K–$Ga_{2.18}$ZnCr	0.90	10.19	7.20	1.04	14.94	13.11

[a] The bulk composition is obtained by the analysis of the XRF of the catalysts. [b] The surface composition is obtained by fitting the spectra of XPS.

recorded. As shown in Fig. S10 and Table S7,† the surface oxygen species are mainly composed of lattice oxygen (O_{latt}) located at 529.5 eV, surface absorbed oxygen (O_{ads}) located at 531.1 eV and absorbed OH groups (O_{OH}) located at 532 eV.[8] O_{ads} and O_{OH} created by the disordered ZnCr catalyst are considered to be the active sites for CO activation and these are advantageous to the formation of a formate group, which is an important C_1 precursor to form C_2 oxygenates. Therefore, the higher the concentration of O_{ads} and O_{OH}, the better the performance of the K–ZnCr catalyst. As listed in Table S7,† the molar ratio of $(O_{ads} + O_{OH})/(O_{latt} + O_{ads} + O_{OH})$ ranged from 36.72% to 46.94%. In addition, the proportion of absorbed OH groups show irregular changes upon increasing the amount of Ga^{3+}, which may be caused by the deduced particle size or the altered interactions between ZnO and $ZnCr_2O_4$. Furthermore, the amount of Ga clusters, ZG and $ZnGa_2O_4$ also changed with the amount of Ga added. This will also influence the basicity and acidity of the catalysts, which is very important for CO activation and iso-butanol formation. The detailed basicity-acidity information about the K–GaZnCr catalyst was investigated using CO_2 and NH_3 TPD and is reported in the following section.

3.8 CO_2-TPD analysis of the basicity of the catalyst samples

In this section, the basicity of the K–GaZnCr iso-butanol catalysts was tested using a CO_2-TPD study, and the results are shown in Fig. S11.† As can be seen from Fig. S11,† all the samples show a remarkable desorption of CO_2 at 170–204 °C, 260–288 °C, 350–367 °C, 440–484 °C and above 600 °C, respectively, corresponding to the different basicity of the catalysts, that is weak basicity, medium basicity, and strong basicity. The CO_2-TPD results demonstrated that the ratios of weak basicity to strong basicity and medium basicity are in the range 0.57–0.47 and 0.64–0.76 for K–Ga_xZnCr (x = 0.0, 0.55, 1.10, and 1.64) and a sharp increase for K–$Ga_{2.18}$ZnCr (0.68 and 1.25), indicating that an excessive amount of Ga^{3+} is harmful to the density of the weak basicity site, but is advantageous to the density of the medium and strong basicity sites, especially to the strong basicity sites. Generally, moderate basicity is important for the carbon chain growth through β-addition during the synthesis of higher alcohol.[14,17,56] If the basicity of the catalyst is too strong, the adsorption of the unsaturated precursors for branched carbon chain growth, for example, propanol or/and formyl group, is so strong that the formation of higher branched carbon chains can not take place.[5,15,16]

3.9 NH_3-TPD analysis of the catalysts

Fig. S12† shows the NH_3-TPD profiles of the K–Ga_xZnCr samples. As shown, all the samples give two major peaks that can be assigned to the weak acidity (around 210 °C) and medium–strong acidity (300–600 °C). The profiles were fitted into five peaks to further investigate the detailed distribution of the acidity. According to the NH_3-TPD profiles, the ratios of weak acidity to medium–strong acidity increased with the increasing amount of Ga^{3+} promoter. As for the medium–strong acidity, K–$Ga_{1.10}$ZnCr shows an identical ratio of medium acidity to strong acidity. The proper ratios of weak to medium–strong acidity and medium to strong acidity play a major part in activating CO and boosting the carbon chain growth during synthesis of higher alcohols.[1] In general, the strong acidity is beneficial to the dissociative absorption of CO, while the weak and medium acidity contribute to the molecular adsorption of CO.[57] Therefore, the moderate acidity is a key role in syngas conversion.

3.10 DRIFTs of CO adsorption on K–Ga_xZnCr catalysts

The adsorption of CO was performed using *in situ* diffuse reflectance infrared Fourier transform spectroscopy (DRIFTS) at 400 °C after H_2 reduction of the K–Ga_xZnCr catalysts. As shown in Fig. S13,† all the samples give the absorption of carbonates located at 1045, 1310 and 1560 cm^{-1} and the absorption of formates located at 1590 and 1610 cm^{-1} respectively.[30,58,59] Moreover, the anti-symmetric stretching vibration of CO_2^- and the symmetric stretching vibration of CH located at 2955, 2865, and 2745 cm^{-1} were also observed.[59] By comparing the intensity of the formate and carbonates located at 1590, 1607, 1045 and 1033 cm^{-1}, one can see that K–$Ga_{0.55}$ZnCr and K–$Ga_{1.10}$ZnCr give a much stronger absorption than the other three samples, indicating that more active sites exist on these two samples. Formate is an important precursor of the C_1 intermediate CHO for the growth of the C–C chain, meanwhile it is also the precursor for forming the OCH_3 group which is the key intermediate to produce methanol.[60] As a result, the higher the concentration of formate, the higher the space time yield (STY) of alcohols that can be expected.

3.11 Performance of the K–GaZnCr catalysts

The typical catalytic performances of the K–Ga_xZnCr catalysts are listed in Table 3. All the evaluation results for the catalysts were collected after 22 h of time on stream in order to minimize the influence of the disturbance by frequent sampling. As can be seen in Table 3, by gradually increasing the amount of Ga^{3+}, the selectivity of CO_2 was decreased from

Table 3 Typical catalytic performance of the K–Ga_xZnCr iso-butanol catalysts

Catalysts	CO conversion, %	STY g h^{-1} g_{cat}^{-1}	Selectivity, C mol%					Distribution of alcohols, wt%				
			CH_4	CO_2	CH_x[a]	DME[b]	Alcohol	MEOH[c]	EtOH[d]	PrOH[e]	i-BuOH[f]	$C^{5+}OH$[g]
K–$Ga_{0.0}$ZnCr	23.59	0.0695	0	42.55	2.95	0	51.50	57.98	0.93	4.38	33.13	3.57
K–$Ga_{0.55}$ZnCr	23.75	0.0996	1.69	38.73	6.70	0.01	52.87	57.23	0.92	3.97	36.03	1.84
K–$Ga_{1.10}$ZnCr	23.17	0.1103	0.85	34.64	5.46	0.01	59.03	59.53	1.02	4.53	31.23	3.69
K–$Ga_{1.64}$ZnCr	21.24	0.1101	1.81	37.23	7.40	0.03	53.72	58.94	0.87	3.96	31.58	4.64
K–$Ga_{2.18}$ZnCr	24.16	0.0819	1.26	34.36	19.96	2.43	41.99	69.44	0.99	4.09	23.21	2.19
K–$ZnGa_2O_4$	14.18	0.0427	1.73	19.53	2.91	58.70	17.13	87.84	1.89	0.53	5.84	1.36

[a] Summary of the amount of ethane, propane and butane in the tail gas. [b] Dimethyl ether. [c] Methanol. [d] Ethanol. [e] *n*-Propanol and isopropanol. [f] Iso-butanol. [g] Amyl alcohol. Reaction conditions: temperature = 400 °C, pressure = 10.0 MPa, GHSV = 3300 h^{-1}.

42.55% for K–Ga_0ZnCr to 34.64% for K$Ga_{1.10}$ZnCr, while the selectivity of the alcohols was increased from 51.50% to 59.03%. In addition, when the amount of Ga^{3+} is lower than 1.64%, the selectivity of methanol and iso-butanol are higher than 57 wt% and 31 wt%, respectively. Upon further increasing the amount of Ga^{3+}, the isobutanol selectivity in the total alcohols was reduced to only 23.21 wt%, while methanol (69.44 wt%) turned out to be the major component of the alcohols. The amount of CH_x and DME were also increased sharply under a higher doping concentration of Ga^{3+}. The evaluation results indicate that the higher concentration of Ga^{3+} has an adverse effect on the performance of the iso-butanol catalyst, which may be attributed to the altered structure of the catalyst. In other words, the main composition of the catalyst is ZnO and $ZnCr_2O_4$ without adding Ga^{3+}. When Ga^{3+} was added, ZG or saturated $ZnCr_2O_4$ were formed. With the gradual addition of Ga^{3+}, the extra ZnO will react with Ga_2O_3 to form $ZnGa_2O_4$ during calcination. Furthermore, the K–$ZnGa_2O_4$ sample was prepared to verify the structure of $ZnGa_2O_4$ and its catalytic performance. The evaluation results show that K–$ZnGa_2O_4$ is probably a DME synthesis catalyst, and this was validated using a K–$Ga_{2.18}$ZnCr sample and only 2.43% DME was obtained, which was much higher than that obtained using the other four catalysts. Thus, the increased amount of DME in K–$Ga_{2.18}$ZnCr indicates the formation of the $ZnGa_2O_4$ species. Other possible reasons, such as the formation of Ga clusters, the interaction of Ga with the coordinately unsaturated $ZnCr_2O_4$ surface will result in the loss of performance of the K–ZnCr catalyst, which was verified by the reduced CO adsorption energy. Moreover, the well-performing K–$Ga_{1.10}$ZnCr catalyst was evaluated using a long-period stability test. The results are shown in Table 4. During 102 h of time on stream, the selectivity of the total alcohol and the fraction of iso-butanol values were found to be above 59% and 31.23 wt% respectively. The STY of the alcohols is in the range of 0.0875–0.1103 g h^{-1} g_{cat}^{-1}, which indicates that the K–$Ga_{1.10}$ZnCr catalyst exhibits a good stability during the reaction.

3.12 Effects of Ga^{3+} on the performance of the K–ZnCr catalyst

In this section, we will further investigate the relationship between the structure of the Ga^{3+} doped catalysts and their performance. To begin with, the possible location of Ga^{3+} was deduced by calculating the E_B and E_f values, as shown in Table S2.† The E_B values for $ZnCr_2O_4$, $ZnGa_2O_4$, ZG, CG, and ZGO follow the order: ZG (348.8783 eV) > $ZnCr_2O_4$ (334.9394 eV) > $ZnGa_2O_4$ (309.8619 eV) > CG (250.3525 eV) > ZGO (19.1836 eV), suggesting that ZG and $ZnCr_2O_4$ are more stable than the other compounds. In addition, the E_r value calculated using their most stable oxides follow the order: $ZnCr_2O_4$ (254.7572 eV) > ZG (243.7237 eV) > $ZnGa_2O_4$ (229.6797 eV) > CG (162.7697 eV), indicating that $ZnCr_2O_4$ and ZG are easier to form through their oxides. As suggested by Li *et al.*, the E_r determines the driving force of a formation

Table 4 The catalytic performance of the K–$Ga_{1.10}$ZnCr iso-butanol catalysts with time on stream

TOS, h	CO conversion, %	STY g h^{-1} g_{cat}^{-1}	Selectivity, C mol%					Distribution of alcohols, wt%				
			CH_4	CO_2	CH_x[a]	DME[b]	Alcohol	MEOH[c]	EtOH[d]	PrOH[e]	i-BuOH[f]	$C^{5+}OH$[g]
22	23.17	0.1103	0.85	34.64	5.46	0.01	59.03	59.53	1.02	4.53	31.23	3.69
31	24.91	0.1000	0.04	34.75	5.18	0.02	60.00	57.28	0.97	4.62	33.44	3.70
46	24.04	0.0955	0	33.77	5.13	0.01	61.08	56.75	1.01	4.52	31.92	5.80
55	23.44	0.1069	0.43	32.13	5.42	0.01	62.00	59.22	1.06	4.57	32.83	2.42
78	29.46	0.0875	0	32.57	4.47	0.01	62.95	58.37	1.02	4.56	33.00	2.96
102	21.34	0.1009	0	35.47	5.15	0.01	59.37	60.75	1.35	4.77	33.13	0

[a] Summary of the amount of ethane, propane and butane in the tail gas. [b] Dimethyl ether. [c] Methanol. [d] Ethanol. [e] *n*-Propanol and isopropanol. [f] Iso-butanol. [g] Amyl alcohol. Reaction conditions: temperature = 400 °C, pressure = 10.0 MPa, GHSV = 3300 h^{-1}.

reaction, a larger E_r will lead to the formation of a more stable compound.[61] By combining the E_r with the E_B, we deduced that the most stable form of the Ga^{3+} doped ZnCr spinel is ZG. The detailed configuration of ZG is listed in the ESI.† The cell parameters of *a*, *b*, and *c* for ZG are 8.3490, 8.3466, and 8.3495 Å, respectively, which are larger than the un-doped ZnCr spinel (a = 8.2300 Å, b = 8.2302 Å, c = 8.32304 Å). The calculated cell parameters are larger than the values that were deduced from the ionic radius of the tetrahedral coordinated Zn^{2+} and Ga^{3+} (their radii are 0.74 and 0. 61 Å, respectively[62]). The difference may be caused by the higher valance of Ga^{3+}. If Zn^{2+} is partly replaced by Ga^{3+}, excessive positive charges need to be neutralized to remain electrically neutral meaning that re-distributions of all cations can be expected, which will induce enlarged cell parameters. Furthermore, when Ga^{3+} was embed in the tetrahedral site of the ZnCr spinel, the Ga–O bond is only about 1.89 Å, which is much shorter than the Ga–O bond located in the Ga_2O_3 crystal (1.94 to 2.10 Å). The calculated Bader charge distributions of Ga for Ga_2O_3, $ZnGa_2O_4$, and ZG are +1.87, +1.83, and +1.77, respectively, suggesting that the electron density of Ga in ZG is higher than the other gallium compounds which may explain the lower BE of Ga 2p in the XPS patterns of the K–GaZnCr catalysts.

Secondly, when ZG was formed, the surface composition of the catalyst was altered. The altered surface composition significantly affected the interaction between ZnO and $ZnCr_2O_4$ which will further impact the ratio of Zn/Cr, and the basicity and acidity of the catalysts. To determine the different surface properties between $ZnCr_2O_4$ and ZG, the $ZnCr_2O_4$ (111) and ZG (111) surfaces were constructed, the adsorption of CO, H_2, H_2O and CO_2 were investigated using DFT calculations. The most stable configurations and adsorption energies of the species are shown in Fig. S14–S17 and Table S8.† The results show that Cr is the most favourable absorption site (Fig. S11†) for CO absorption on both the $ZnCr_2O_4$ (111) and ZG (111) surfaces. The absorption energies are −0.74 and −2.99 eV respectively, which indicate that Ga^{3+} adoption is helpful to the absorption of CO. In addition, remarkably decreased adsorption energies for CO_2 and H_2O on the ZG (111) surface were also observed (Table S6†), suggesting that CO_2 and H_2O are not favourable for absorption on the ZG (111) surface. During syngas conversion, the water gas shift reaction (WGSR) is an inevitable reaction that consumes a large amount of CO and thus reduces the efficiency of carbon resource usage. Hence, it is important to reduce or suppress this reaction. The smaller absorption energy of H_2O indicates that it is not easy for H_2O to participate in the WGSR to produce CO_2. This is firmly verified by the evaluation results of the K–Ga_xZnCr catalyst.

Thirdly, the productivity of hydrocarbons such as ethane and propane increased with the increasing amount of Ga^{3+}, that is from 2.95% for K–$Ga_{0.0}$ZnCr to 19.96% for K–$Ga_{2.18}$-ZnCr. Although Cryder *et al.* proposed that the excess of surface chromium oxides gives rise to the amount of CO_2 and hydrocarbons,[63] we conclude that the hydrocarbons in the gas product are mainly caused by the presence of the ZG compound. The reason for this lies in the following two aspects: (i) the ratios of Zn/Cr on the surface of the samples are almost the same for the K–Ga_xZnCr (x = 0, 0.55, 1.10, 1.64, and 2.18) samples, as detected by XPS, therefore the effects of extra chromium on the selectivity of the hydrocarbons can be excluded. (ii) CO is easier to dissociate on the ZG (111) surface than on the $ZnCr_2O_4$ (111) surface, which can be verified using the CI-NEB calculation on the elementary reaction CO═C + O. The results show that the activation energy for CO dissociation is 3.32 eV lower on the ZG (111) surface than on the $ZnCr_2O_4$ (111) surface (shown in Fig. S18A†). The dissociated CO is considered to be the origin of the CH_x species, leading to the formation of hydrocarbons on the samples with a higher amount of added Ga^{3+}.

Finally, the formation of CHO by CO hydrogenation was also studied on the different catalyst surfaces to investigate the influence of the surface structure on the CHO formation. CHO is regarded as an important intermediate to participate in the formation of the first C_2 oxygenates, which is the rate determining step for higher alcohol synthesis. In addition, CHO is also the precursor of the OCH_3 group, and then by step by step hydrogenation, methanol will be produced. Therefore, the higher the concentration of CHO, the higher the selectivity of alcohol is expected. Lower values for the activation energy and reaction energy were obtained using DFT calculations, for example 0.96 and 0.24 eV on the ZnCr spinel (111) surface *versus* 0.78 and −1.05 eV on the ZG (111) surface (Fig. S18B†). The reduced activation energy and reaction energy for CHO formation indicate that Ga^{3+} adsorption is advantageous to the formation of CHO, which will further boost the selectivity of the alcohols.

Conclusions

Ga^{3+} promoted K–ZnCr catalysts were prepared using the precipitation–impregnation method. The optimal K–$Ga_{1.10}$-ZnCr catalyst shows a 58.70% increase in the STY and a 14.62% promotion on the selectivity of the alcohols under the reaction conditions of 10.0 MPa, 400 °C and 3300 h^{-1} GHSV. Spectral analysis and first principles calculations revealed that the Zn^{2+} ions, located at the tetrahedral site of the ZnCr spinel, were replaced by Ga^{3+} ions to form the ZG structure, which promoted the direct dissociation of CO and the formation of the CHO group. The coordinately unsaturated $ZnCr_2O_4$ surfaces interacted with Ga or gallium clusters which reduced the adsorption of CO along with this process. However, upon further increasing the amount of Ga^{3+}, $ZnGa_2O_4$ was formed which would modulate the morphologies, surface acidity and basicity of the final catalysts, eventually inducing the poor performance of the catalysts.

Conflicts of interest

The authors declare no competing financial interests.

Acknowledgements

This work is supported by the National Natural Science Foundation of China (21573269). Financial aid from the Fund Program for the Scientific Activities of Selected Returned Overseas Professionals in Shanxi Province, China is also greatly appreciated. The DFT calculations were performed on the Tianhe-II HPC at the Lvliang HPC Centre, China. The authors give special thanks for the foundations and computational resource support provided by the government and the company.

References

1 M. Ao, G. H. Pham, J. Sunarso, M. O. Tade and S. Liu, *ACS Catal.*, 2018, **8**, 7025–7050.
2 H. Guo, S. Li, H. Zhang, F. Peng, L. Xiong, J. Yang, C. Wang, X. Chen and Y. Chen, *Ind. Eng. Chem. Res.*, 2014, **53**, 123–131.
3 K. A. N. Verkerk, B. Jaeger, C.-H. Finkeldei and W. Keim, *Appl. Catal., A*, 1999, **186**, 407–431.
4 H. T. Luk, C. Mondelli, D. C. Ferre, J. A. Stewart and J. Perez-Ramirez, *Chem. Soc. Rev.*, 2017, **46**, 1358–1426.
5 Y. Wu, N. Gong, M. Zhang, W. Zhang, T. Zhang, J. Zhang, L. Wang, H. Xie and Y. Tan, *Catal. Sci. Technol.*, 2019, **9**, 2592–2600.
6 S. Gao, X. Li, Y. Li, H. Yu, F. Zhang, Y. Sun, H. Fang, X. Zhang, X. Liang and Y. Yuan, *Fuel*, 2018, **230**, 194–201.
7 S. Tian, L. Tan, Y. Wu, Y. Kou, H. Xie, N. Tsubaki and Y. Tan, *Appl. Catal., A*, 2017, **536**, 57–66.
8 S. Tian, S. Wang, Y. Wu, J. Gao, P. Wang, H. Xie, G. Yang, Y. Han and Y. Tan, *Catal. Sci. Technol.*, 2016, **6**, 4105–4115.
9 L. Tan, G. Yang, Y. Yoneyama, Y. Kou, Y. Tan, T. Vitidsant and N. Tsubaki, *Appl. Catal., A*, 2015, **505**, 141–149.
10 S. Tian, S. Wang, Y. Wu, J. Gao, Y. Bai, P. Wang, H. Xie, Y. Han and Y. Tan, *J. Mol. Catal. A: Chem.*, 2015, **404**, 139–147.
11 X. Gao, Y. Wu, T. Zhang, L. Wang, X. Li, H. Xie and Y. Tan, *Catal. Sci. Technol.*, 2018, **8**, 2975–2986.
12 X. Gao, T. Zhang, Y. Wu, G. Yang, M.-H. Tan, L. Xiaoli, H. Xie, J. Pan and Y. Tan, *Fuel*, 2018, **217**, 21–30.
13 L. Wang, X. Gao, Y. Bai, M. Tan, K. Sun, T. Zhang, Y. Wu, J. Pan, H. Xie and Y. Tan, *Fuel*, 2019, **253**, 1570–1577.
14 K. J. Smith and R. B. Anderson, *J. Catal.*, 1984, **85**, 428–436.
15 K. J. Smith and R. B. Anderson, *J. Catal.*, 1984, **85**, 428–436.
16 L. Lietti, E. Tronconi and P. Forzatti, *J. Catal.*, 1992, **135**, 400–419.
17 Y. Wu, H. Xie, Y. Kou, N. Tsubaki, Y. Han and Y. Tan, *Korean J. Chem. Eng.*, 2015, **32**, 406–412.
18 W. S. Epling, G. B. Hoflund and D. M. Minahan, *Appl. Catal., A*, 1999, **183**, 335–343.
19 D. M. Minahan, W. S. Epling and G. B. Hoflund, *J. Catal.*, 1998, **179**, 241–257.
20 W. S. Epling, G. B. Hoflund and D. M. Minahan, *J. Catal.*, 1998, **175**, 175–184.
21 W. S. Epling, G. B. Hoflund and D. M. Minahan, *React. Kinet. Catal. Lett.*, 1999, **67**, 225–232.
22 Z. An, X. Ning and J. He, *J. Catal.*, 2017, **356**, 157–164.
23 A. Venugopal, J. Palgunadi, J. K. Deog, O.-S. Joo and C.-H. Shin, *J. Mol. Catal. A: Chem.*, 2009, **302**, 20–27.
24 S.-H. Kang, J. W. Bae, P. S. S. Prasad, J.-H. Oh, K.-W. Jun, S.-L. Song and K.-S. Min, *J. Ind. Eng. Chem.*, 2009, **15**, 665–669.
25 K. Sun, Y. Wu, M. Tan, L. Wang, G. Yang, M. Zhang, W. Zhang and Y. Tan, *ChemCatChem*, 2019, **11**, 2695–2706.
26 A. R. Kim, B. Lee, M. J. Park, D. J. Moon and J. W. Bae, *Catal. Commun.*, 2012, **19**, 66–69.
27 M. M.-J. Li, Z. Zeng, F. Liao, X. Hong and S. C. E. Tsang, *J. Catal.*, 2016, **343**, 157–167.
28 Y.-x. Pan, P. Kuai, Y. Liu, Q. Ge and C.-j. Liu, *Energy Environ. Sci.*, 2010, **3**, 1322–1325.
29 H. Ham, S. W. Baek, C.-H. Shin and J. W. Bae, *ACS Catal.*, 2019, **9**, 679–690.
30 T. Zhang, Y. Wu, X. Gao, H. Xie, G. Yang, N. Tsubaki and Y. Tan, *Fuel*, 2019, **237**, 1021–1028.
31 L. Lutterotti, M. Bortolotti, G. Ischia, I. Lonardelli and H.-R. Wenk, *Z. Kristallogr. Suppl.*, 2007, **26**, 125–130.
32 L. Lutterotti, *Nucl. Instrum. Methods Phys. Res., Sect. B*, 2010, **268**, 334–340.
33 L. Lutterotti, D. Chateigner, S. Ferrari and J. Ricote, *Thin Solid Films*, 2004, **450**, 34–41.
34 L. Lutterotti, S. Matthies, H. R. Wenk, A. S. Schultz and J. W. Richardson, *J. Appl. Phys.*, 1997, **81**, 594–600.
35 C. Vargas-Hernández, O. Almanza and J. F. Jurado, *J. Phys.: Conf. Ser.*, 2009, **167**, 012037.
36 S. Tian, S. Wang, Y. Wu, J. Gao, Y. Bai, P. Wang, H. Xie, Y. Han and Y. Tan, *J. Mol. Catal. A: Chem.*, 2015, **404–405**, 139–147.
37 H. Song, D. Laudenschleger, J. J. Carey, H. Ruland, M. Nolan and M. Muhler, *ACS Catal.*, 2017, **7**, 7610–7622.
38 T. Pandiyarajan, M. L. Baesso and B. Karthikeyan, *Eur. Phys. J. D*, 2014, **68**(28), 1–8.
39 J. Wang, L. Ye, X. Wang, H. Zhang, L. Li, C. Kong and W. Li, *J. Alloys Compd.*, 2019, **803**, 9–15.
40 X. Lu, Z. Du, B. Quan, W. Bian, H. Zhu and Q. Zhang, *J. Mater. Chem. C*, 2019, **7**, 8261–8268.
41 C. Cristiani, P. Forzatti and M. Bellotto, *J. Chem. Soc., Faraday Trans. 1*, 1989, **85**(4), 895–906.
42 M. M. Can, G. H. Jaffari, S. Aksoy, S. I. Shah and T. Firat, *J. Alloys Compd.*, 2013, **549**, 303–307.
43 R. S. Weber, *J. Catal.*, 1995, **151**, 470–474.
44 H. Tajizadegan, A. Heidary, O. Torabi, M. H. Golabgir and A. Jamshidi, *Int. J. Appl. Ceram. Technol.*, 2015, **13**(2), 289–294.
45 H. Lin, C. P. Huang, W. Li, C. Ni, S. I. Shah and Y.-H. Tseng, *Appl. Catal., B*, 2006, **68**, 1–11.
46 O. Nishimura, K. Yabe and M. Iwaki, *J. Electron Spectrosc. Relat. Phenom.*, 1989, **49**, 335–342.
47 R. Merryfield, M. McDaniel and G. Parks, *J. Catal.*, 1982, **77**, 348–359.
48 P. Delichere, S. Daniele and L. G. Hubert-Pfalzgraf, *Surf. Sci. Spectra*, 2001, **8**, 303–311.
49 M. Chen, P. Wu, Q. Wei, Y. Zhu, S. Yang, L. Ju, N. Zhu and Z. Lin, *Environ. Chem.*, 2018, **15**, 226–235.

50 H. Fan, G. Wang and L. Hu, *Solid State Sci.*, 2009, **11**, 2065–2070.
51 X. Duan, F. Yu and Y. Wu, *Eur. J. Inorg. Chem.*, 2013, 1287–1293, DOI: 10.1002/ejic.201201004.
52 N. Li, P. Zhu and X. Duan, *Phys. B*, 2018, **530**, 290–294.
53 C. Han, W. Mao, K. Bao, H. Xie, Z. Jia and L. Ye, *Int. J. Hydrogen Energy*, 2017, **42**, 19913–19919.
54 N. C. Jeong, J. S. Lee, E. L. Tae, Y. J. Lee and K. B. Yoon, *Angew. Chem., Int. Ed.*, 2008, **47**, 10128–10132.
55 W. Yang, J. Li, X. Zhang, C. Zhang, X. Jiang and B. Liu, *Inorg. Chem.*, 2019, **58**, 549–556.
56 T. J. Mazanec, *J. Catal.*, 1986, **98**, 115–125.
57 B. T. Loveless, C. Buda, M. Neurock and E. Iglesia, *J. Am. Chem. Soc.*, 2013, **135**, 6107–6121.
58 M. D. Rhodes, K. A. Pokrovski and A. T. Bell, *J. Catal.*, 2005, **233**, 210–220.
59 A. Riva, F. Trifirò, A. Vaccari, L. Mintchev and G. Busca, *J. Chem. Soc., Faraday Trans. 1*, 1988, **84**(5), 1423–1435.
60 L. C. Grabow and M. Mavrikakis, *ACS Catal.*, 2011, **1**, 365–384.
61 Y. Li, F. Lian, N. Chen, Z.-J. Hao and K.-C. Chou, *Int. J. Miner., Metall. Mater.*, 2015, **22**, 524–529.
62 J. U. Brehm, M. Winterer and H. Hahn, *J. Appl. Phys.*, 2006, **100**, 9.
63 D. S. Cryder and P. K. Frolich, *Ind. Eng. Chem.*, 1929, **21**, 867–871.

